NANO LETTERS
Cite This: Nano Lett. 2018, 18, 2545−2550
Letter
pubs.acs.org/NanoLett

Hot Hole Collection and Photoelectrochemical CO_2 Reduction with Plasmonic Au/p-GaN Photocathodes

Joseph S. DuChene,[†,‡,§] Giulia Tagliabue,[†,‡,§] Alex J. Welch,[†,‡] Wen-Hui Cheng,[†,‡] and Harry A. Atwater*[,†,‡]

[†]Thomas J. Watson Laboratory of Applied Physics and [‡]Joint Center for Artificial Photosynthesis, California Institute of Technology, Pasadena, California 91125 United States

Supporting Information

ABSTRACT: Harvesting nonequilibrium hot carriers from plasmonic-metal nanostructures offers unique opportunities for driving photochemical reactions at the nanoscale. Despite numerous examples of hot electron-driven processes, the realization of plasmonic systems capable of harvesting hot holes from metal nanostructures has eluded the nascent field of plasmonic photocatalysis. Here, we fabricate gold/p-type gallium nitride (Au/p-GaN) Schottky junctions tailored for photoelectrochemical studies of plasmon-induced hot-hole capture and conversion. Despite the presence of an interfacial Schottky barrier to hot-hole injection of more than 1 eV across the Au/p-GaN heterojunction, plasmonic Au/p-GaN photocathodes exhibit photoelectrochemical properties consistent with the injection of hot holes from Au nanoparticles into p-GaN upon plasmon excitation. The photocurrent action spectrum of the plasmonic photocathodes faithfully follows the surface plasmon resonance absorption spectrum of the Au nanoparticles and open-circuit voltage studies demonstrate a sustained photovoltage during plasmon excitation. Comparison with Ohmic Au/p-NiO heterojunctions confirms that the vast majority of hot holes generated via interband transitions in Au are sufficiently hot to inject above the 1.1 eV interfacial Schottky barrier at the Au/p-GaN heterojunction. We further investigated plasmon-driven photoelectrochemical CO_2 reduction with the Au/p-GaN photocathodes and observed improved selectivity for CO production over H_2 evolution in aqueous electrolytes. Taken together, our results offer experimental validation of photoexcited hot holes more than 1 eV below the Au Fermi level and demonstrate a photoelectrochemical platform for harvesting hot carriers to drive solar-to-fuel energy conversion.

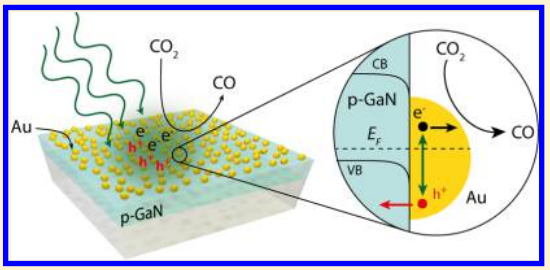

KEYWORDS: *Photoelectrochemistry, hot carriers, plasmonic photocathode, CO_2 reduction, Schottky barrier, hot holes*

The generation of nonequilibrium "hot" electron−hole pairs via surface plasmon decay within metal nanostructures holds great promise for initiating and controlling chemical reactions at the nanoscale.[1−6] However, the capture and conversion of photoexcited hot carriers presents challenges, given their very short mean-free paths (l_{mfp} ∼ 2−20 nm) and excited-state lifetimes (t ∼ fs−ps).[7−15] Hot carrier collection schemes typically involve the formation of an interfacial Schottky barrier (Φ_B) between plasmonic metals (e.g., Au) and wide band gap semiconductors (e.g., n-type TiO_2) to quickly capture hot electrons in a plasmonic photosensitization strategy similar to that employed in dye-sensitized solar cells (Figure 1a). Although numerous optoelectronic systems have been devised to harness plasmonic hot electrons for sub-band gap photodetection[16−21] and plasmon-driven photocatalysis,[22−32] little is known about hot holes derived from surface plasmon decay. Recent theoretical calculations have predicted an asymmetry in the energy distributions between hot electrons and hot holes relative to the metal Fermi level (E_F) in common plasmonic metals like Au and Cu.[8−12] Because of the high density of electronic d-band states, photoexcitation above the interband threshold of the metal (d-band to sp-band transition) can generate hot holes that are much "hotter" (further away from the Fermi level) than hot electrons (Figure 1b).[8−12] In Au nanostructures, an imbalance in hot carrier distributions would be expected to occur for photon energies $h\nu$ > 1.8 eV.[8] Resonant optical excitation of the dipole plasmon mode in spherical Au nanoparticles ($h\nu$ ∼ 2.4 eV) should therefore preferentially produce hot holes within the Au d-band that reside far below the Au Fermi level.[8−12,33] This substantial asymmetry between the energy distributions of hot carriers implies a greater collection efficiency of hot holes relative to hot electrons for a comparable Schottky barrier height (Figure 1). The strong oxidizing power of these hot d-band holes also offers the potential for driving various oxidation reactions if they could be transferred to an appropriate catalyst. Indeed, photo-oxidation of adsorbed citrate molecules in the plasmon-driven synthesis of colloidal Ag and Au nanoprisms is known to proceed more efficiently via "hot" d-band holes as compared to "warm" sp-band holes.[34−39] Strategies that can efficiently and selectively harvest hot holes from metal nanostructures would

Received: January 18, 2018
Revised: February 28, 2018
Published: March 9, 2018

DOI: 10.1021/acs.nanolett.8b00241
Nano Lett. 2018, 18, 2545−2550

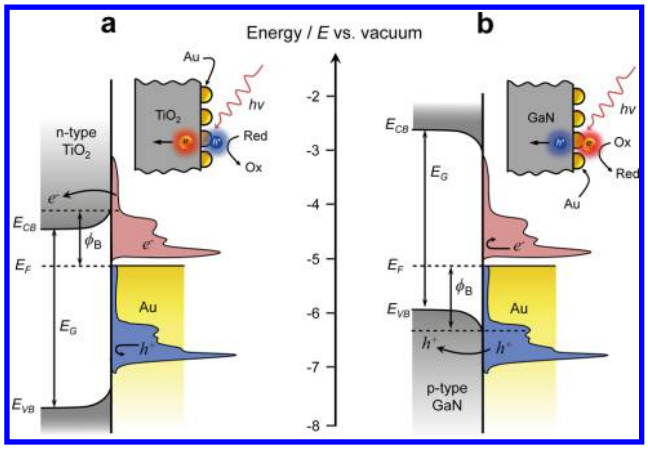

Figure 1. Hot carrier collection across an interfacial Schottky barrier at metal/semiconductor heterojunctions. (a) Energy band diagram of a plasmonic metal (e.g., Au) in physical contact with an n-type semiconductor (e.g., TiO_2), depicting the conduction band edge (E_{CB}), valence band edge (E_{VB}), band gap (E_G), Fermi level (E_F), and the interfacial Schottky barrier (Φ_B). Plasmon excitation creates hot electrons (red) and hot holes (blue) above and below the E_F of Au, respectively, with a distribution of energies governed by the metal band structure and the incident photon energy ($h\nu$ = 2.4 eV). Only those hot electrons with sufficient energies above Φ_B (indicated by dashed line) can surmount the interfacial barrier and populate available CB levels of the n-type semiconductor support. (b) Energy band diagram of a plasmonic metal (e.g., Au) in physical contact with a p-type semiconductor (e.g., p-GaN), depicting E_{CB}, E_{VB}, E_G, E_F, and Φ_B. Plasmon excitation creates hot electrons (red) and hot holes (blue) above and below the E_F of Au, respectively. Only those hot holes with sufficient energies below Φ_B (indicated by dashed line) can surmount the interfacial barrier and populate available VB levels of the p-type semiconductor support.

therefore offer significant benefits for plasmonic photochemistry.[40−42]

To date, however, nearly all studies of hot carrier collection have focused on the capture and conversion of hot electrons with n-type semiconductors (Figure 1a). Comparatively fewer studies have examined the sensitization of wide band gap p-type semiconductors, in which the plasmonic metal injects hot holes directly into the valence band of an adjoining p-type semiconductor support (Figure 1b). Such a plasmonic photosensitization scheme would enable adsorbed molecules to harvest hot electrons directly from metal nanostructures while obviating the need for sacrificial reagents that are often used to facilitate charge separation. Despite much promise, harvesting hot holes from metal nanostructures is more challenging than hot electron collection, given the relatively short mean-free path (l_{mfp} ~ 5−10 nm) of hot holes 1−2 eV below the E_F compared to hot electrons 1−2 eV above the E_F (l_{mfp} ~ 20 nm).[8−11] There are also far fewer wide band gap p-type semiconductors available for sensitization than n-type semiconductors. Although p-type nickel oxide (p-NiO) has been shown to serve as a carrier-selective contact for hot-hole collection from photoexcited Au nanoparticles,[43,44] the absence of a suitable Schottky barrier at the Au-NiO interface permits the collection of holes from the metal Fermi level down to the photon energy ($E_F - h\nu$). Such a system is therefore incapable of selectively probing the population of "hot" holes generated deep below the metal Fermi level upon plasmon excitation. As a result, the energy distribution and associated prevalence of hot holes in metal nanostructures upon photoexcitation is not well understood.

Here, we employ p-type gallium nitride (p-GaN) as a semiconductor support for photoelectrochemical studies of hot-hole collection from Au nanoparticles. As a wide band gap (E_g ~ 3.4 eV) semiconductor that exhibits p-type conductivity, p-GaN is an ideal semiconductor support for investigating hot-hole collection above the interband threshold of a plasmonic nanoantenna. Importantly, the sizable Schottky barrier (Φ_B > 1 eV) established across the Au/p-GaN interface provides a suitable platform for probing the existence of very hot holes deep below the metal Fermi level upon photoexcitation of Au nanoparticles. Our photoelectrochemical studies show that plasmonic Au/p-GaN photocathodes indeed support cathodic photocurrents consistent with the collection of plasmon-induced holes that are more than 1 eV below the Au Fermi level and the measured action spectrum faithfully follows the surface plasmon resonance of the Au nanoparticles. Significantly, open-circuit voltage measurements demonstrate a sustained plasmonic photovoltage across the metal−semiconductor heterojunction whose sign is consistent with the injection of hot holes into the p-GaN support. We further used these Au/p-GaN photocathodes for plasmon-driven CO_2 reduction, demonstrating the utility of these plasmonic photocathodes for artificial photosynthesis. These results demonstrate the feasibility of harvesting hot holes from plasmonic-metal nanostructures and open a route for the design of plasmonic photocathodes that can capture visible light to drive photochemistry.

Plasmonic Au/p-GaN photocathodes (Figure 2a) were synthesized by electron-beam physical vapor deposition of Au nanoparticles onto epitaxial p-type GaN (*c*-axis 0001 orientation, Pam-Xiamen) grown on sapphire (see Methods). The bare GaN-on-sapphire substrate is optically transparent and displays a direct optical band gap of ca. 3.35 eV (Figure S1), consistent with the 3.4 eV band gap expected for GaN.[45−48] The wide band gap of p-GaN ensures that any visible-light response observed at photon energies below 3.4 eV from the Au/p-GaN device can be attributed to hot-hole injection from the Au nanoparticles. Scanning electron microscopy (SEM) shows Au nanoparticles of diameter d = 8.2 ± 1.6 nm uniformly distributed across the p-type GaN surface after briefly annealing in ambient air at 300 °C for 1 h (Figure 2a,b). The absence of stabilizing surfactants and molecular linkers is advantageous for establishing direct physical contact at the Au/p-GaN interface while also exposing a clean Au surface for catalysis. It is further noted that no adhesion layer is required to construct the metal−semiconductor heterojunction, excluding any possible contribution from interfacial metal layers on the device operation. The Au/p-GaN substrate adopts a purple color and exhibits a prominent absorption peak in the visible region at about 570 nm, attributable to the surface plasmon resonance of Au nanoparticles (Figure 2c, red curve). The fringes present in both absorption spectra are due to Fabry-Pérot interferences within the high-index GaN layer.

Solid-state electrical measurements were conducted to verify that a Schottky barrier (Φ_B) was established across the Au/p-GaN interface (see Methods). Ohmic contacts to the p-GaN substrate were fabricated according to previous literature protocols[49,50] via codeposition of a 10 nm thick Ni/Au (50/50 atomic %) alloy followed by annealing in ambient air for 1 h at 500 °C. A metal−semiconductor Schottky junction was then

DOI: 10.1021/acs.nanolett.8b00241
Nano Lett. 2018, 18, 2545−2550

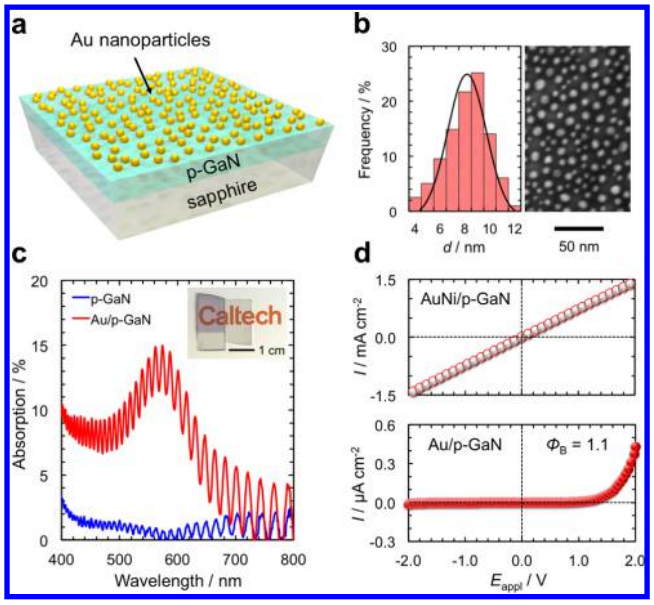

Figure 2. Plasmonic Au/p-GaN photocathode device structure. (a) Schematic of Au/p-GaN photocathode on sapphire substrate. (b) SEM image with corresponding size-distribution histogram of Au nanoparticles (mean diameter d = 8.2 ± 1.6 nm) on p-GaN substrate. (c) Absorption spectra of plasmonic Au/p-GaN photocathode (red curve) compared to bare p-GaN substrate (blue curve). The plasmonic device shows a prominent surface plasmon resonance feature due to the Au nanoparticles at ca. 570 nm. Inset shows a digital photograph of the colorless p-GaN substrate and the purple Au/p-GaN device. (d) Solid-state current−voltage (I−E_{appl}) behavior from Au/p-GaN heterostructures. Ohmic contact to the p-GaN substrate was achieved through deposition of a thin-film Au/Ni alloy (top panel). In contrast, a metal−semiconductor Schottky diode was obtained across the Au/p-GaN heterojunction (bottom panel). Fitting of these data yields a Schottky barrier height of Φ_B = 1.1 eV across the Au/p-GaN interface.

constructed from 100 nm thick Au contacts. Electrical measurements were conducted under an optical microscope using piezoelectric microprobes to electrically address the contact pads on the p-GaN substrate. As shown in Figure 2d (top panel), Ohmic behavior was observed when both probes were electrically connected to the Ni/Au alloy contacts. In contrast, rectifying device characteristics were observed when one of the microprobes was moved onto the Au contact pad (Figure 2d, bottom panel). Fitting of these data to the diode equation yields a Schottky barrier height of Φ_B = 1.1 eV across the Au/p-GaN heterojunction, similar to the 1.2 eV barrier previously observed for Au/p-GaN contacts.[51] The Au/p-GaN photocathode therefore provides a suitable photoelectrochemical platform to probe the production of hot holes with energies in excess of 1 eV in Au nanoparticles.

Photoelectrochemical studies were performed using a potentiostat in a three-electrode configuration with the Au/p-GaN photocathode as working electrode, a platinum wire mesh counter electrode, and a saturated calomel electrode (SCE) as the reference electrode. The electrolyte (50 mM K_2CO_3) was sparged with N_2 gas for 30 min prior to experiments, which were performed under a N_2 blanket. All electrochemical potentials are reported with respect to the reversible hydrogen electrode (RHE). Mott−Schottky analysis of electrochemical impedance data obtained at 2 kHz confirms the p-type conductivity of the bare GaN films (Figure S2). From a linear fit of the data, we obtained a carrier concentration of about 1 × 10^{19} cm^{-3}, similar to the acceptor doping level of N_A = 3−7 × 10^{18} cm^{-3} specified by the manufacturer. The flat-band potential (E_{fb}) is about 2.0 V_{RHE} (V vs RHE), consistent with prior reports.[45−47] We estimate the width of the depletion region (W_d) within the p-GaN substrate to be between 11−20 nm, implying that hot-hole tunneling through the barrier can be neglected. Any hot holes collected by the underlying p-GaN support upon plasmon excitation must therefore possess sufficient energy to surmount the ∼1 eV Schottky barrier at the metal−semiconductor interface.

The potential−current (E−J) behavior of the plasmonic photocathode was assessed via linear sweep voltammetry under periodic (0.5 Hz), visible-light excitation (λ > 495 nm) at a scan rate of 10 mV s^{-1} to simultaneously monitor the dark current (J) and the photocurrent (J_{ph}). As shown in Figure 3a (red curve), the Au/p-GaN device displayed cathodic photocurrents (J_{ph}) along the potential sweep consistent with the collection of hot holes across the metal−semiconductor heterojunction. The Au/p-GaN photocathode exhibits an onset potential (E_{on}) of about 0.4 V_{RHE} and attained a J_{ph} of 1.8 μA cm^{-2} at −0.8 V_{RHE}. Cyclic voltammograms of bare p-GaN and Au/p-GaN photocathodes under dark and light conditions are shown in Figure S3. The bare p-GaN photocathode exhibits no discernible J_{ph} response under visible-light excitation across the entire potential sweep (Figure 3a, blue curve and Figure

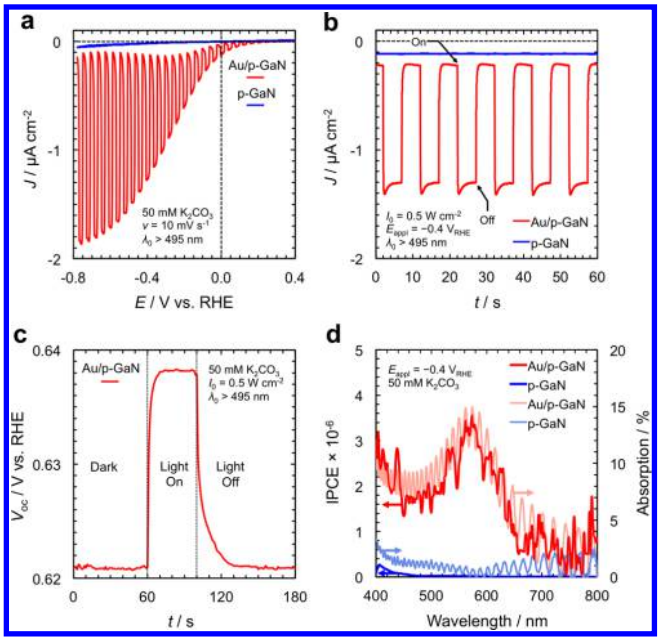

Figure 3. Photoelectrochemical characterization of plasmonic Au/p-GaN photocathodes. (a) Linear sweep voltammetry of plasmonic Au/p-GaN (red) and bare p-GaN (blue) photocathodes at 10 mV s^{-1} under periodic (0.5 Hz), visible-light irradiation (λ > 495 nm) at an incident power of I_0 = 600 mW cm^{-2}. (b) Chronoamperometry of plasmonic Au/p-GaN (red) and bare p-GaN (blue) photocathodes under periodic (0.5 Hz), visible-light irradiation (λ > 495 nm) while poised at a fixed applied potential of −0.4 V_{RHE}. (c) Chronopotentiometry of the open-circuit voltage (V_{oc}) from plasmonic Au/p-GaN photocathodes under visible-light irradiation. (d) IPCE of plasmonic Au/p-GaN (red) and bare p-GaN (blue) photocathodes immersed in 50 mM K_2CO_3 electrolyte while held at a fixed potential of −0.4 V_{RHE}. The absorption spectra of each device are also plotted with the IPCE spectra to aid comparison between photoelectrochemical performance and light absorption.

DOI: 10.1021/acs.nanolett.8b00241
Nano Lett. 2018, 18, 2545−2550

S3). Chronoamperometry $J(t)$ experiments were then performed with the plasmonic photocathode poised at −0.4 V_{RHE}. As shown in Figure 3b, the plasmonic Au/p-GaN device exhibits a prompt and reproducible cathodic J_{ph} of 1.3 μA cm^{-2} under periodic, visible-light illumination (λ > 495 nm). For comparison, no visible light response was observed from the bare p-GaN support under otherwise identical experimental conditions (Figure 3b, blue curve). As expected for a hot carrier-driven process,[52] the plasmonic photocathode exhibits a linear J_{ph} response with respect to incident light power (Figure S4).

Plasmon-driven charge separation across the Au/p-GaN interface was examined by monitoring the open-circuit voltage (V_{oc}) of the device under visible-light excitation (λ > 495 nm). For a p-type semiconductor in contact with an aqueous electrolyte, Fermi level equilibration between the semiconductor (E_F) and the redox species in the electrolyte ($E_{F,Redox}$ = E_F) establishes a depletion region within the semiconductor that results in downward band-bending near the surface.[47] Upon optical excitation, the electric field across the space-charge layer draws photogenerated electrons to the semiconductor−liquid junction where they are scavenged by redox species in the electrolyte (e.g., protons), leaving behind charge vacancies (i.e., holes) to accumulate within the bulk of the semiconductor. This accumulation of holes causes a downward shift of their quasi-Fermi level ($E_{F,p}$) with respect to the dark equilibrium level (E_F), driving the V_{oc} of the p-type photocathode to more positive values.[47] Indeed, band gap excitation of bare p-GaN photocathodes with UV light induces a positive shift in the V_{oc} of the device (Figure S5). As there are no free electrons photogenerated directly within the p-GaN conduction band upon illumination with sub-band gap visible light, any changes in the V_{oc} of the Au/p-GaN photocathode can be attributed to the injection of hot holes into the p-GaN valence band. Thus, monitoring changes in the V_{oc} of the Au/p-GaN photocathode upon plasmon excitation enables the detection of hot hole injection across the metal−semiconductor heterojunction in the absence of an applied electrical bias, E_{appl}. The Au/p-GaN photocathode was allowed to equilibrate with the electrolyte for several hours in the dark until a steady V_{oc} baseline was obtained ($V_{oc,dark}$ = 0.62 V_{RHE}). Plasmon excitation of the Au nanoparticles promptly drives the injection of hot holes into the p-GaN support (Figure 3c), as evidenced by the positive shift of V_{oc} upon the incidence of visible light ($V_{oc,light}$ = 0.64 V_{RHE}). A plasmonic photovoltage (V_{ph} = $V_{oc,light}$ − $V_{oc,dark}$) of about 20 mV was eventually established within the photocathode and sustained over 30 s before the light was turned off. The hot holes present in the p-GaN valence band must then recombine across the Au/p-GaN interface to re-establish the equilibrium V_{oc} obtained under dark conditions. The observation of a plasmonic photovoltage demonstrates the ability to maintain charge separation across the Schottky barrier at the Au/p-GaN interface under steady-state operation.

The photoelectrochemical action spectrum, $J_{ph}(\lambda)$, was assessed via incident photon-to-current conversion efficiency (IPCE) measurements with the photocathode poised at −0.4 V_{RHE} in 50 mM K_2CO_3 electrolyte. Figure 3d shows that the IPCE of the plasmonic photocathode (red curve) faithfully follows the surface plasmon resonance of the Au nanoparticles (light red curve) across the visible regime. For comparison, no J_{ph} response is observed from the bare p-GaN device under otherwise identical experimental conditions (Figure 3d, blue curve). Taken together, these photoelectrochemical data confirm that the visible-light response observed from the Au/p-GaN device is derived from hot-hole injection upon plasmon excitation of the Au nanoparticles. Given the considerable Schottky barrier height at the Au/p-GaN interface (Φ_B = 1.1 eV), such a result is encouraging for the design of optoelectronic devices that operate via the collection of hot holes from metal nanostructures.

The influence of interfacial barrier height on hot-hole collection from Au nanoparticles was then investigated through the construction and evaluation of a plasmonic photocathode composed of Au nanoparticles on p-type nickel oxide (p-NiO) films (see Methods). As a wide band gap semiconductor that natively exhibits p-type conductivity and forms an Ohmic contact with Au,[44] plasmonic Au/p-NiO photocathodes offer a complementary photoelectrochemical system for assessing the collection of hot holes from Au nanoparticles in the absence of an interfacial barrier (Figure S6a−d). Au nanoparticles of about 10 ± 1 nm in diameter were uniformly decorated onto the p-NiO surface in the same way as for the Au/p-GaN device (Figure S6e). The Au/p-NiO photocathodes exhibit a surface plasmon resonance feature at about 560 nm with nearly identical overall magnitude as the Au/p-GaN system (Figure S6f). Solid-state I−V measurements confirm Ohmic contact between Au nanoparticles and the p-NiO film (Figure S7a). Chronoamperometry of Au/p-NiO photocathodes yielded photocurrents of 2.7 μA cm^{-2} at −0.4 V_{RHE} under periodic, visible-light irradiation (λ > 495 nm), while no J_{ph} response was obtained from the bare p-NiO substrate (Figure S7b). The incident photon-to-charge conversion efficiency (IPCE) $J_{ph}(\lambda)$ of Au/p-NiO qualitatively follows the surface plasmon resonance of the Au nanoparticles, indicating that all photocurrent is attributable to hot-hole injection from Au nanoparticles to the p-NiO support (Figure S7c). The striking similarity in photoelectrochemical performance between Au/p-NiO (2.7 μA cm^{-2} at −0.4 V_{RHE}) and Au/p-GaN (1.3 μA cm^{-2} at −0.4 V_{RHE}) indicates that the vast majority of hot holes generated in the Au/p-GaN device are sufficiently hot to inject above the 1.1 eV interfacial Schottky barrier at the Au/p-GaN heterojunction. This experimental result is consistent with prior theoretical predictions of the hot-hole distribution generated on Au nanoparticles upon photoexcitation above the interband threshold of the metal.[8−11] Considering the vast difference in barrier height between these two material systems (∼1 eV), such a result is promising for the eventual exploitation of plasmon-derived hot holes for solar photochemistry.

To that end, Au/p-GaN photocathodes were employed for plasmon-driven carbon dioxide (CO_2) reduction in CO_2-saturated 50 mM K_2CO_3 electrolyte in a three-electrode configuration with Pt gauze as the counter electrode and a SCE as the reference electrode. No sacrificial reagents were used in the reaction. The photocathode was potentiostatically poised at −1.8 V_{RHE} while the reactor headspace gas was periodically sampled and analyzed via gas chromatography over a 48 h period (see Methods). It has previously been reported that p-GaN nanowires, which predominantly expose m-planes, produce carbon monoxide (CO), hydrogen (H_2), and methane (CH_4) in the absence of a metal cocatalyst.[53] Under our experimental conditions, we find that the bare p-GaN substrate (c-plane) produces primarily H_2 and CO, with trace amounts of CH_4 under dark electrolysis (Figure S8). The bare p-GaN surface exhibits a substantial preference for proton reduction over CO_2 reduction, evolving H_2 at a rate that is about 3.5 times greater than CO. In contrast, the addition of Au

DOI: 10.1021/acs.nanolett.8b00241
Nano Lett. 2018, 18, 2545−2550

nanoparticles substantially alters the selectivity of the device for CO_2 reduction. Under dark electrolysis, the Au/p-GaN device exhibits improved selectivity for CO_2 reduction to CO with a significant reduction in H_2 evolution relative to the bare p-GaN surface (Figure 4a). From these data, the Au/p-GaN device

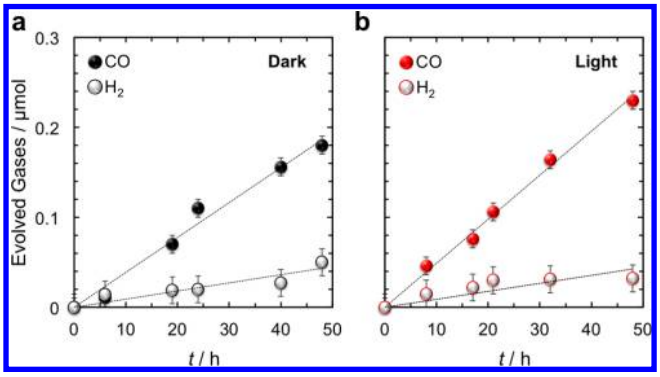

Figure 4. Photoelectrochemical CO_2 reduction with plasmonic Au/p-GaN photocathodes. (a) Time-course of gas evolution from plasmonic Au/p-GaN photocathode during controlled potential electrolysis under dark conditions. (b) Time-course of gas evolution from plasmonic Au/p-GaN photocathode during controlled potential electrolysis under plasmon excitation (λ > 495 nm). All electrolysis experiments were performed at −1.8 V_{RHE} in CO_2-saturated 50 mM K_2CO_3 electrolyte without sacrificial reagents.

produces CO-to-H_2 at a ratio of about 4:1 under dark conditions. Plasmon excitation of the Au nanoparticles with visible light (λ > 495 nm) was found to increase the CO evolution rate by 20%, from about 4 nmol h^{-1} in the dark to about 5 nmol h^{-1} in the light, while exerting little influence on the rate of H_2 evolution (Figure 4b). Plasmonic Au/p-GaN photocathodes therefore exhibit improved selectivity for photoelectrochemical CO_2 reduction in aqueous electrolytes, producing CO-to-H_2 at a ratio of 5:1 upon plasmon excitation (Figure 4b). The photoelectrochemical stability of these plasmonic photocathodes is evidenced by the continuous evolution of gaseous products over 96 h of electrochemical operation. Overall, these results are consistent with recent experimental observations of improved selectivity for plasmon-driven CO_2 reduction with plasmonic-metal nanostructures[25,30] and demonstrate the utility of plasmonic photocathodes for artificial photosynthesis.

In summary, we have demonstrated the collection of plasmon-induced hot holes from Au nanoparticles via construction of an interfacial Schottky barrier with p-type GaN. Although the photocurrents reported here are relatively modest ($\sim\mu$A cm^{-2}), substantial enhancements in device performance may be achievable by implementing this photosensitization scheme for p-GaN nanowire arrays to dramatically increase the available surface area for light collection and catalysis.[54−57] Further improvements could also be realized through roughening the metal−semiconductor interface to relieve the momentum matching restrictions for hot hole transmission across planar metal−semiconductor Schottky junctions investigated here. More broadly, the realization of a plasmon-driven photocathode capable of collecting hot holes at least 1.1 eV below the Au Fermi level holds tantalizing prospects for plasmonic photochemistry, given the considerable oxidizing power of such carriers. These results support previous observations of plasmon-driven water oxidation with Au nanoparticles[58−60] and suggest room for further improvements if the hot holes could be efficiently transferred to an appropriate catalyst. Further studies are needed to fully elucidate the factors governing plasmonic hot hole collection in p-type semiconductor systems along with their associated carrier dynamics. Though at an early stage, our demonstration of a plasmon-driven artificial photosynthetic system for CO_2 conversion offers promise for the eventual exploitation of both hot electrons and hot holes in fuel-forming photochemical reactions.

■ ASSOCIATED CONTENT

Supporting Information

The Supporting Information is available free of charge on the ACS Publications website at DOI: 10.1021/acs.nanolett.8b00241.

Detailed experimental methods, optical properties of p-GaN films, cyclic voltammograms of Au/p-GaN and p-GaN photocathodes, open-circuit voltage of p-GaN photocathodes, materials characterization of p-NiO films, optoelectronic and photoelectrochemical characterization of Au/p-NiO photocathodes, gas chromatography results from bare p-GaN photocathodes (PDF)

■ AUTHOR INFORMATION

Corresponding Author

*E-mail: haa@caltech.edu.

ORCID

Joseph S. DuChene: 0000-0002-7145-323X

Harry A. Atwater: 0000-0001-9435-0201

Author Contributions

J.S.D., G.T., and H.A.A. conceived the idea, designed the experiments, and wrote the manuscript. J.S.D. and G.T. performed all photoelectrochemical experiments. J.S.D., G.T., and A.J.W. fabricated devices. W.-H.C. performed optical characterization and assisted with gas chromatography experiments. H.A.A. supervised the project. All authors have given approval to the final version of the manuscript.

Notes

The authors declare no competing financial interest.

§J.S.D. and G.T. contributed equally to this work.

■ ACKNOWLEDGMENTS

This material is based upon work performed by the Joint Center for Artificial Photosynthesis, a DOE Energy Innovation Hub, supported through the Office of Science of the U.S. Department of Energy under Award No. DE-SC0004993. G.T. acknowledges support from the Swiss National Science Foundation through the Early Postdoc Mobility Fellowship, Grant P2EZP2_159101 and the Advanced Mobility Fellowship, Grant P300P2_171417. We thank Dr. Ravishankar Sundararaman, Dr. Prineha Narang, and Adam Jermyn for fruitful discussions of hot-carrier energy distributions. We thank Dr. Matthias Richter for XPS characterization of p-type NiO films.

■ REFERENCES

(1) Linic, S.; Christopher, P.; Ingram, D. B. *Nat. Mater.* **2011**, *10*, 911−921.

(2) Clavero, C. *Nat. Photonics* **2014**, *8*, 95−103.

(3) Brongersma, M. L.; Halas, N. J.; Nordlander, P. *Nat. Nanotechnol.* **2015**, *10*, 25−34.

DOI: 10.1021/acs.nanolett.8b00241
Nano Lett. 2018, 18, 2545−2550

(4) Christopher, P.; Moskovits, M. *Annu. Rev. Phys. Chem.* **2017**, *68*, 379−398.
(5) Linic, S.; Aslam, U.; Boerigter, C.; Morabito, M. *Nat. Mater.* **2015**, *14*, 567−576.
(6) Hartland, G. V.; Besteiro, L. V.; Johns, P.; Govorov, A. O. *ACS Energy Lett.* **2017**, *2*, 1641−1653.
(7) Manjavacas, A.; Liu, J. G.; Kulkarni, V.; Nordlander, P. *ACS Nano* **2014**, *8*, 7630−7638.
(8) Brown, A. M.; Sundararaman, R.; Narang, P.; Goddard, W. A., III; Atwater, H. A. *ACS Nano* **2016**, *10*, 957−966.
(9) Sundararaman, R.; Narang, P.; Jermyn, A. S.; Goddard, W. A., III; Atwater, H. A. *Nat. Commun.* **2014**, *5*, 5788.
(10) Bernardi, M.; Mustafa, J.; Neaton, J. B.; Louie, S. G. *Nat. Commun.* **2015**, *6*, 7044.
(11) Govorov, A. O.; Zhang, H.; Gun'ko, Y. K. *J. Phys. Chem. C* **2013**, *117*, 16616−16631.
(12) Liu, J. G.; Zhang, H.; Link, S.; Nordlander, P. *ACS Photonics* **2017**, DOI: 10.1021/acsphotonics.7b00881.
(13) Harutyunyan, H.; Martinson, B. F. A.; Rosenmann, D.; Khorashad, L. K.; Besteiro, L. V.; Govorov, A. O.; Wiederrecht, G. P. *Nat. Nanotechnol.* **2015**, *10*, 770−774.
(14) Hartland, G. V. *Chem. Rev.* **2011**, *111*, 3858−3887.
(15) Brown, A. M.; Sundararaman, R.; Narang, P.; Schwartzberg, A. M.; Goddard, W. A., III; Atwater, H. A. *Phys. Rev. B* **2017**, *118*, 087401.
(16) Knight, M. W.; Sobhani, H.; Nordlander, P.; Halas, N. J. *Science* **2011**, *332*, 702−704.
(17) Zheng, B. Y.; Zhao, H.; Manjavacas, A.; McClain, M.; Nordlander, P.; Halas, N. J. *Nat. Commun.* **2015**, *6*, 7797.
(18) Li, W.; Valentine, J. *Nano Lett.* **2014**, *14*, 3510−3514.
(19) Goykhman, I.; Desiatov, B.; Khurgin, J.; Shappir, J.; Levy, U. *Nano Lett.* **2011**, *11*, 2219−2224.
(20) Chalabi, H.; Schoen, D.; Brongersma, M. L. *Nano Lett.* **2014**, *14*, 1374−1380.
(21) Li, W.; Coppens, Z. J.; Besteiro, L. V.; Wang, W.; Govorov, A. O.; Valentine, J. *Nat. Commun.* **2015**, *6*, 8379.
(22) Mubeen, S.; Hernandez-Sosa, G.; Moses, D.; Lee, J.; Moskovits, M. *Nano Lett.* **2011**, *11*, 5548−5552.
(23) Mubeen, S.; Lee, J.; Singh, N.; Kramer, S.; Stucky, G. D.; Moskovits, M. *Nat. Nanotechnol.* **2013**, *8*, 247−251.
(24) Mubeen, S.; Lee, J.; Liu, D.; Stucky, G. D.; Moskovits, M. *Nano Lett.* **2015**, *15*, 2132−2136.
(25) Robatjazi, H.; Zhao, H.; Swearer, D. F.; Hogan, N. J.; Zhou, L.; Alabastri, A.; McClain, M. J.; Nordlander, P.; Halas, N. J. *Nat. Commun.* **2017**, *8*, 27.
(26) Swearer, D. F.; Zhao, H.; Zhou, L.; Zhang, C.; Robatjazi, H.; Martirez, J. M. P.; Krauter, C. M.; Yazdi, S.; McClain, M. J.; Ringe, E.; Carter, E. A.; Nordlander, P.; Halas, N. J. *Proc. Natl. Acad. Sci. U. S. A.* **2016**, *113*, 8916−8920.
(27) Mukherjee, S.; Zhou, L.; Goodman, A. M.; Large, N.; Ayala-Orozco, C.; Zhang, Y.; Nordlander, P.; Halas, N. J. *J. Am. Chem. Soc.* **2014**, *136*, 64−67.
(28) Zhou, L.; Zhang, C.; McClain, M. J.; Manjavacas, A.; Krauter, C. M.; Shu, T.; Berg, F.; Everitt, H. O.; Carter, E. A.; Nordlander, P.; Halas, N. J. *Nano Lett.* **2016**, *16*, 1478−1484.
(29) Zhang, C.; Zhao, H.; Zhou, L.; Schlather, A. E.; Dong, L.; McClain, M. J.; Swearer, D. F.; Nordlander, P.; Halas, N. J. *Nano Lett.* **2016**, *16*, 6677−6682.
(30) Zhang, X.; Li, X.; Zhang, D.; Su, N. Q.; Yang, W.; Everitt, H. O.; Liu, J. *Nat. Commun.* **2017**, *8*, 14542.
(31) Aslam, U.; Chavez, S.; Linic, S. *Nat. Nanotechnol.* **2017**, *12*, 1000−1005.
(32) Zhong, Y.; Ueno, K.; Mori, Y.; Shi, X.; Oshikiri, T.; Murakoshi, K.; Inoue, H.; Misawa, H. *Angew. Chem., Int. Ed.* **2014**, *53*, 10350−10354.
(33) Sá, J.; Tagliabue, G.; Friedli, P.; Szlachetko, J.; Rittmann-Frank, M. H.; Santomauro, F. G.; Milne, C. J.; Sigg, H. *Energy Environ. Sci.* **2013**, *6*, 3584−3588.
(34) Thrall, E. S.; Steinberg, A. P.; Wu, X.; Brus, L. E. *J. Phys. Chem. C* **2013**, *117*, 26238−26247.
(35) Langille, M. R.; Personick, M. L.; Mirkin, C. A. *Angew. Chem., Int. Ed.* **2013**, *52*, 13910−13940.
(36) Wu, X.; Redmond, P. L.; Liu, H.; Chen, Y.; Steigerwald, M.; Brus, L. *J. Am. Chem. Soc.* **2008**, *130*, 9500−9506.
(37) Schlather, A. E.; Manjavacas, A.; Lauchner, A.; Marangoni, V. S.; DeSantis, C. J.; Nordlander, P.; Halas, N. J. *J. Phys. Chem. Lett.* **2017**, *8*, 2060−2067.
(38) Wu, X.; Thrall, E. S.; Liu, H.; Steigerwald, M.; Brus, L. *J. Phys. Chem. C* **2010**, *114*, 12896−12899.
(39) Zhai, Y.; DuChene, J. S.; Wang, Y.-C.; Qiu, J.; Johnston-Peck, A. C.; You, B.; Guo, W.; DiCiaccio, B.; Qian, K.; Zhao, E. W.; Ooi, F.; Hu, D.; Su, D.; Stach, E. A.; Zhu, Z.; Wei, D. W. *Nat. Mater.* **2016**, *15*, 889−895.
(40) Zhao, J.; Nguyen, S. C.; Ye, R.; Ye, B.; Weller, H.; Somorjai, G. A.; Alivisatos, A. P.; Toste, F. D. *ACS Cent. Sci.* **2017**, *3*, 482−488.
(41) Kim, Y.; Torres, D. D.; Jain, P. K. *Nano Lett.* **2016**, *16*, 3399−3407.
(42) Moskovits, M. *Nat. Nanotechnol.* **2015**, *10*, 6−8.
(43) Nakamura, K.; Oshikiri, T.; Ueno, K.; Wang, Y.; Kamata, Y.; Kotake, Y.; Misawa, H. *J. Phys. Chem. Lett.* **2016**, *7*, 1004−1009.
(44) Robatjazi, H.; Bahauddin, S. M.; Doiron, C.; Thomann, I. *Nano Lett.* **2015**, *15*, 6155−6161.
(45) Beach, J. D.; Collins, R. T.; Turner, J. A. *J. Electrochem. Soc.* **2003**, *150*, A899−A904.
(46) Kibria, M. G.; Mi, Z. *J. Mater. Chem. A* **2016**, *4*, 2801−2820.
(47) Kamimura, J.; Bogdanoff, P.; Ramsteiner, M.; Corfdir, P.; Feix, F.; Geelhaar, L.; Riechert, H. *Nano Lett.* **2017**, *17*, 1529−1537.
(48) Kibria, M. G.; Chowdhury, F. A.; Zhao, S.; Al Oltaibi, B.; Trudeau, M. L.; Guo, H.; Mi, Z. *Nat. Commun.* **2015**, *6*, 6797.
(49) Ho, J.-K.; Jong, C.-S.; Chiu, C. C.; Huang, C.-N.; Shih, K.-K.; et al. *J. Appl. Phys.* **1999**, *86*, 4491−4497.
(50) Jang, H. W.; Kim, S. Y.; Lee, J.-L. *J. Appl. Phys.* **2003**, *94*, 1748−1752.
(51) Wu, C. I.; Kahn, A. *J. Vac. Sci. Technol., B: Microelectron. Process. Phenom.* **1998**, *16*, 2218−2223.
(52) Christopher, P.; Xin, H.; Linic, S. *Nat. Chem.* **2011**, *3*, 467−472.
(53) Al Otaibi, B.; Fan, S.; Wang, D.; Ye, J.; Mi, Z. *ACS Catal.* **2015**, *5*, 5342−5348.
(54) Boettcher, S. W.; Spurgeon, J. M.; Putnam, M. C.; Warren, E. L.; Turner-Evans, D. B.; Kelzenberg, M. D.; Maiolo, J. R.; Atwater, H. A.; Lewis, N. S. *Science* **2010**, *327*, 185−187.
(55) Kelzenberg, M. D.; Boettcher, S. W.; Petykiewicz, J. A.; Turner-Evans, D. B.; Putnam, M. C.; Warren, E. L.; Spurgeon, J. M.; Briggs, R. M.; Lewis, N. S.; Atwater, H. A. *Nat. Mater.* **2010**, *9*, 239−244.
(56) Wang, D.; Pierre, A.; Kibria, M. G.; Cui, K.; Han, X.; Bevan, K. H.; Guo, H.; Paradis, S.; Hakima, A.-R.; Mi, Z. *Nano Lett.* **2011**, *11*, 2353−2357.
(57) Al Otaibi, B.; Nguyen, H. P. T.; Zhao, S.; Kibria, M. G.; Fan, S.; Mi, Z. *Nano Lett.* **2013**, *13*, 4356−4361.
(58) Shi, X.; Ueno, K.; Takabayashi, N.; Misawa, H. *J. Phys. Chem. C* **2013**, *117*, 2494−2499.
(59) Nishijima, Y.; Ueno, K.; Kotake, Y.; Murakoshi, K.; Inoue, H.; Misawa, H. *J. Phys. Chem. Lett.* **2012**, *3*, 1248−1252.
(60) Wang, S.; Gao, Y.; Miao, S.; Liu, T.; Mu, L.; Li, R.; Fan, F.; Li, C. *J. Am. Chem. Soc.* **2017**, *139*, 11771−11778.

DOI: 10.1021/acs.nanolett.8b00241
Nano Lett. 2018, 18, 2545−2550